MgO Layer Thickness Dependence of Structure and Magnetic Properties of $L1_0$-FePt/MgO/GaAs Structures

Japanese Journal of Applied Physics **51** (2012) 02BM05 **REGULAR PAPER**
DOI: 10.1143/JJAP.51.02BM05

MgO Layer Thickness Dependence of Structure and Magnetic Properties of $L1_0$-FePt/MgO/GaAs Structures

Rento Ohsugi[1], Makoto Kohda[1,2*], Takeshi Seki[3], Akihiko Ohtsu[1], Masaki Mizuguchi[3], Koki Takanashi[3], and Junsaku Nitta[1]

[1]*Department of Materials Science, Tohoku University, Sendai 980-8579, Japan*
[2]*PRESTO, Japan Science and Technology Agency, Kawaguchi, Saitama 332-0012, Japan*
[3]*Institute for Materials Research, Tohoku University, Sendai 980-8577, Japan*

Received October 3, 2011; accepted October 18, 2011; published online February 20, 2012

We investigated the MgO layer thickness dependences of the structure and magnetic properties of $L1_0$-FePt/MgO/GaAs structures. To examine how the crystallinity and growth morphology of the MgO layer affect the $L1_0$-FePt layer, two kinds of preparation method were employed for MgO deposition: electron beam (EB) evaporation and sputter deposition. The MgO layer deposited by EB evaporation included a large strain because of the cube-on-cube epitaxial relationship despite a large lattice mismatch between MgO and GaAs. For the MgO layer prepared by sputtering, on the other hand, an amorphous MgO layer was initially grown on the GaAs substrate. Subsequently, a crystalline MgO layer was grown in the (001) direction. In the case of the EB-deposited MgO, as the MgO layer thickness increased, the degree of chemical order of the $L1_0$-FePt layer increased from 55 to 81% owing to the improvement of the crystallinity of the MgO layer. The improvement of chemical order also led to the increase in the remanent magnetization of $L1_0$-FePt from 84 to 98%.

1. Introduction

A ferromagnetic metal (FM)/semiconductor (SC) heterostructure is one of the important building blocks for operating spintronic devices at room temperature. Electrical spin injection into an SC through a high-quality heterojunction is a fundamental requirement for FM/SC heterostructures. Recently, nonlocal spin injection and detection have been achieved in FM/SC structures such as Fe/GaAs[1)] and CoFe/GaAs.[2)] In these devices, however, an easy magnetization axis of ferromagnetic metal electrodes was aligned in the in-plane direction owing to the demagnetizing field. To utilize the spin degree of freedom by taking advantage of spin orbit interaction for an electrical spin manipulation[3)] and a reduced threshold current in a vertical-cavity surface-emitting laser,[4)] a perpendicularly magnetized FM/SC structure is indispensable. An $L1_0$-FePt alloy is one of the promising materials for injecting perpendicularly oriented electron spins at zero magnetic field because $L1_0$-FePt shows large perpendicular magnetic anisotropy.[5,6)] In addition to this, an $L1_0$-FePt layer is directly grown on a MgO layer, which means that MgO is utilized as a tunnel barrier for the efficient spin injection into an SC. By taking advantage of this feature, an electrical spin injection from $L1_0$-FePt into GaAs has been demonstrated at room temperature.[7)] However, the remanent magnetization of $L1_0$-FePt is low, resulting in a low spin injection efficiency at zero magnetic field. In a previous study, we grew $L1_0$-FePt/MgO/GaAs structures with a high remanent magnetization with a sputtered MgO tunnel barrier layer.[8)] However, the qualities of the MgO layer and the interface between MgO and GaAs have not been fully understood. It is essential to confirm and improve the interface quality for an efficient spin injection.

In this study, we have investigated the MgO thickness dependences of the magnetic properties of the $L1_0$-FePt layer in $L1_0$-FePt/MgO/GaAs structures. Two kinds of preparation technique were employed for MgO deposition: electron beam (EB) deposition and sputter deposition. The structural difference has also been compared between EB-deposited MgO and sputtered MgO.

*E-mail address: makoto@material.tohoku.ac.jp

Table I. Thickness of the FePt and MgO layers (in nm) for sputtered MgO and EB-deposited MgO samples.

	FePt thickness	MgO thickness
Sputtered MgO samples	5	3
		5
EB-deposited MgO samples	20	2
		3
		5

2. Sample Preparation and Growth Condition

To obtain a clean surface of GaAs (001) substrates, the GaAs (001) substrates were cleaned in $HCl : H_2O = 1 : 1$ liquid for 2 min to remove oxides and –OH on their surface. After cleaning, the GaAs substrates were immediately transferred into the prechamber and annealed for 10 min in vacuum at a substrate temperature (T_S) of 400 °C. For the MgO growth, we employed two different methods: the magnetron sputtering and the EB evaporation. The T_S value of the sputtered MgO and EB-deposited MgO layers were 350 and 400 °C, respectively. After the MgO growth, samples were transferred into an ultrahigh-vacuum sputtering chamber without breaking the vacuum condition. Then, Fe and Pt were co-sputtered on the MgO layer with $Fe_{0.43}Pt_{0.57}$ composition. The T_S value during the FePt growth were 350 °C for sputtered MgO samples and 400 °C for EB-deposited MgO samples.

Table I shows a summary of the thicknesses of FePt and MgO layers for all the samples. To monitor the flatness and the growth direction of each layer, we used the reflection high energy electron diffraction (RHEED). Structural analyses of the $L1_0$-ordered FePt/MgO/GaAs film were performed by θ–2θ X-ray diffraction (XRD) measurement. XRD measurement was performed with Cu Kα radiation, and its step of 2θ was fixed at 0.04°. To observe the morphology of $L1_0$-FePt/MgO/GaAs interfaces, we conducted the cross-sectional transmission electron microscopy (TEM). The magnetic properties of $L1_0$-FePt layers were measured using the polar magneto-optical Kerr effect

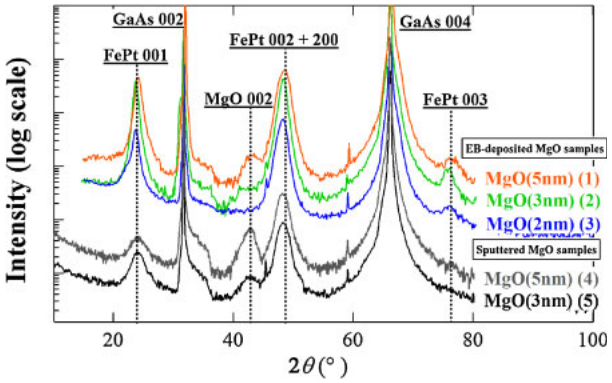

Fig. 1. (Color online) (a) XRD patterns of EB-deposited MgO samples with (1) 5, (2) 3, and (3) 2 nm MgO thickness and of sputtered MgO samples with (4) 5 and (5) 3 nm MgO thickness.

(PMOKE) with application of the external magnetic field normal to the film plane.

To calculate the degree of chemical order parameter S of $L1_0$-FePt, we used the following equation:

$$\sqrt{\left(\frac{A_{001}}{A_{002}}\right)\Big/\left(\frac{A_{001}}{A_{002}}\right)_{\text{theory}}} = S,$$

where A_{001} and A_{002} are the integrated intensities of the 001 superlattice and 002 fundamental peaks in XRD measurement, respectively. $(A_{001}/A_{002})_{\text{theory}}$ is the theoretical ratio of A_{001} to A_{002} for the fully ordered alloy at $Fe_{0.43}Pt_{0.57}$ composition, which is 0.38.

3. Results and Discussion

From the XRD patterns of FePt/MgO/GaAs structures shown in Fig. 1, a clear MgO 002 peak appears with increasing MgO layer thickness, indicating the (001) orientation of the MgO layer on the GaAs (001) substrate. In addition to the FePt 002 fundamental peak, the FePt 001 and FePt 003 superlattice peaks are observed for all the samples. It is found that the $L1_0$-ordered FePt (001) layer was grown on (001) MgO/(001) GaAs by both EB deposition and sputtering processes. RHEED patterns are also shown in the insets in Fig. 2(b). These clear streak patterns indicate the flat surface of each layer. From the results of XRD and RHEED measurements, the cube-on-cube epitaxial relationship of $[100]_{GaAs} \parallel [100]_{MgO} \parallel [100]_{FePt}$ and $(001)_{GaAs} \parallel (001)_{MgO} \parallel (001)_{FePt}$ is found in the EB-deposited MgO sample.

To examine the morphology of interfaces in the $L1_0$-FePt/MgO/GaAs structures, cross-sectional TEM was performed. Figures 2(a) and 2(b) show the TEM images of $L1_0$-FePt/MgO/GaAs structures with a sputtered MgO layer and an EB-deposited MgO layer, respectively. As shown in Fig. 2(a), a thin amorphous MgO layer is observed at the MgO/GaAs interface of the sputtered MgO samples, and a crystalline MgO (001) texture is subsequently grown after the formation of the amorphous MgO layer. The in-plane crystal orientation of the MgO layer grown on the amorphous layer is not confined, unlike that of the MgO layer epitaxially grown on GaAs. In the case of the EB-deposited MgO sample [Figs. 2(b) and 2(c)], on the other hand, there is no formation of an amorphous layer at the interface. The

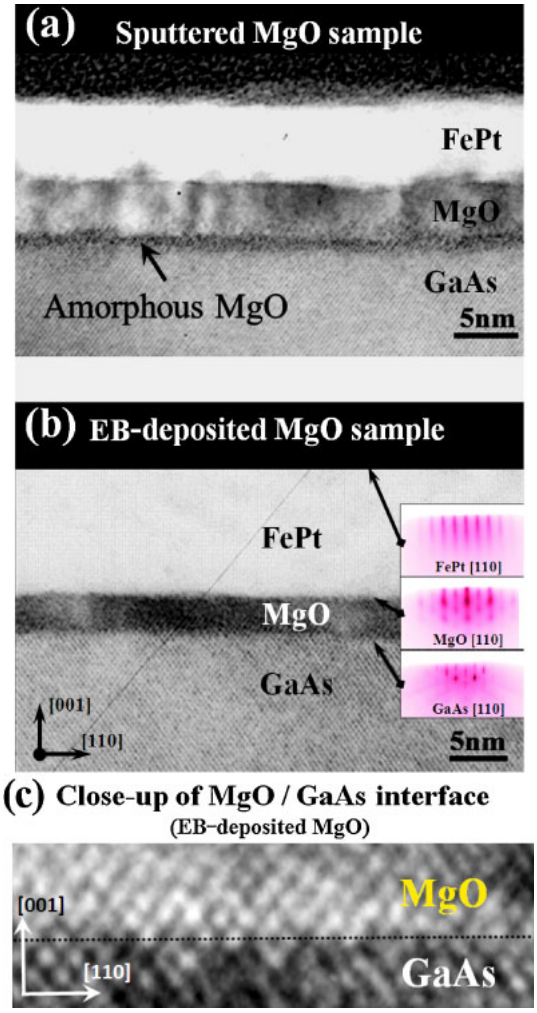

Fig. 2. (Color online) Cross-sectional TEM images of $L1_0$-FePt/MgO/GaAs structure. (a) $L1_0$-FePt (5 nm)/sputtered MgO (5 nm)/GaAs sample. (b) $L1_0$-FePt (20 nm)/EB-deposited MgO (3 nm)/GaAs sample. (c) MgO and GaAs interface in EB-deposited MgO sample.

Table II. Lattice constant and FWHM in sputtered MgO and EB-deposited MgO layers evaluated from the MgO 002 peaks obtained from XRD measurement.

	C-axis lattice constant (Å)	FWHM (deg)
Sputtered MgO (5 nm)	4.213	1.055
EB-deposited MgO (5 nm)	4.200	2.170

root-mean-square roughness values of FePt/MgO interfaces are calculated to be 0.62 and 0.19 nm for the sputtered and EB-deposited MgO samples, respectively. The EB-deposited MgO sample has a flat FePt/MgO interface compared with the sputtered MgO sample.

Since the lattice mismatch between MgO (4.213 Å) and GaAs (5.68 Å) is over 25%, the cube-on-cube epitaxial relationship could lead to a large strain accumulation in the MgO layer, which gives rise to a large dispersion of crystal orientation. To understand the strain accumulation in EB-deposited MgO layer and sputtered MgO layer, the full widths at half maximum (FWHMs) of MgO 002 peaks are evaluated.

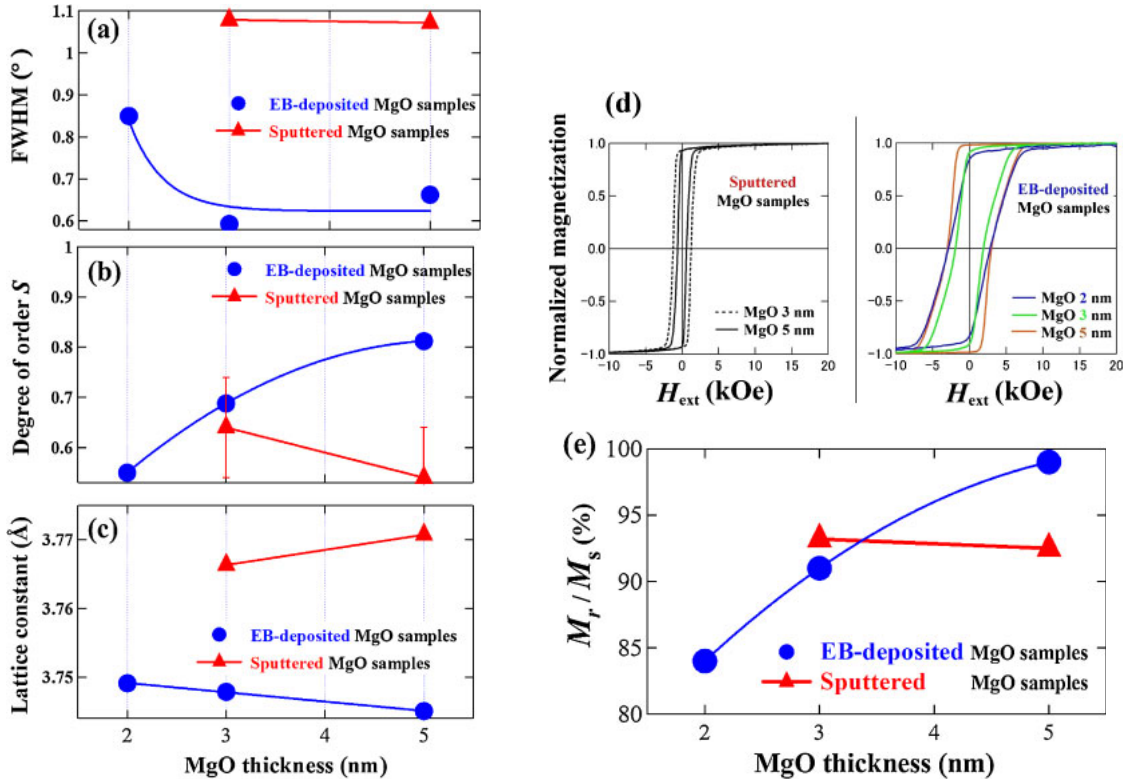

Fig. 3. (Color online) (a) FWHMs of FePt 002 peaks, (b) degree of chemical order parameters S of $L1_0$-FePt, (c) c-axis lattice constants, (d) PMOKE(M-H) loops of both sputtered (left side) and EB-deposited (right side) MgO samples, and (e) remanent magnetization M_r/M_s.

Table II shows the c-axis lattice constants of the MgO layers and FWHMs of MgO 002 peaks. The c-axis lattice constants for both MgO layers are almost identical to each other, the values of which are consistent with the bulk lattice constant of MgO (4.213 Å). However, the FWHM of the EB-deposited 5 nm MgO layer (2.170°) is twice larger than that of the sputtered 5 nm MgO layer (1.055°). Such a peak broadening of MgO 002 indicates the large dispersion of the c-axis orientation for the EB-deposited MgO layer. This difference in dispersions of crystal orientation between the EB-deposited and sputtered samples results from the different growth morphologies at the MgO/GaAs interface. In the case of the sputtered MgO layer, the formation of the amorphous MgO layer excludes the strain accumulation at the MgO/GaAs interface, and the subsequent crystalline MgO layer formation results in the narrow XRD peaks. On the other hand, the EB-deposited MgO layer has large strain accumulation due to the epitaxial growth without the formation of the amorphous MgO layer, leading to the large FWHM.

To understand the effect of the strain at the MgO/GaAs interface on the magnetic properties of $L1_0$-FePt, the MgO layer thickness dependences of the FWHM of the FePt 001 peak are evaluated for EB-deposited MgO samples as well as sputtered MgO samples. Figure 3(a) shows the FWHMs of FePt 001 peaks as a function of the MgO layer thickness. With increasing MgO layer thickness, the FWHM of FePt decreases in the case of the EB-deposited MgO samples. This implies that the dispersion of crystal orientation of the MgO layer affected the c-axis distribution of the FePt layer. The thick MgO layer improves the crystallinity of the FePt layer. On the other hand, there is no change in the FWHM of the sputtered MgO samples owing to the exclusion of the strain accumulation by the amorphous MgO layer. The strain due to the lattice mismatch affects the magnetic properties of $L1_0$-FePt.[6)]

Figures 3(b) and 3(c) show the degree of chemical order parameters S and c-axis lattice constants of the FePt layers, respectively. For the EB-deposited MgO samples, when the MgO layer thickness increases, S increases from 0.55 to 0.81, whereas the c-axis lattice constant decreases. Since the c-axis of the FePt is reduced when the FePt transforms from the disorder (fcc) phase to the order ($L1_0$) phase,[5)] the increase in S is in agreement with the decrease in the c-axis lattice constant of FePt. One of the reasons for the promotion of $L1_0$-ordering is the improvement of the crystallinity of the FePt layer with the thick MgO layer. The c-axis lattice constants of FePt in sputtered MgO samples are larger than that in EB-deposited MgO samples, because the absence of strain accumulation in the sputtered MgO layer leads to a smaller a-axis than in the case of the EB-deposited MgO layer.

Figure 3(d) shows the PMOKE loops for FePt layers prepared on the sputtered MgO and EB-deposited MgO layers. All the films show high remanent magnetization in the perpendicular direction, indicating the existence of perpendicular magnetic anisotropy. However, the ratio of remanent magnetization to saturation magnetization (M_r/M_s) gradually changes depending on the MgO layer thickness. Figure 3(e) shows M_r/M_s as a function of the MgO layer thickness of the sputtered MgO and EB-deposited MgO samples. For the EB-deposited MgO samples, M_r/M_s increases from 84 to 98% with increasing MgO layer thickness. The increase in M_r/M_s is consistent

with the MgO layer thickness dependence of S. For the sputtered MgO samples, M_r/M_s does not show a marked change with MgO layer thickness. This tendency is interpreted as being due to the fact that the strain is not accumulated in the MgO (001) layer due to the formation of the amorphous MgO layer on the GaAs surface.

4. Conclusions

We investigated the MgO layer thickness dependences of the structure and magnetic properties of $L1_0$-FePt on MgO/GaAs structures. The MgO layers prepared by EB evaporation epitaxially grew on the GaAs (100) substrate while the sputtered MgO layer initially formed an amorphous MgO on the GaAs surface. The cube-on-cube epitaxial relationship gave rise to a large strain in the EB-deposited MgO layer, and the magnetic properties of $L1_0$-FePt changed with increasing MgO layer thickness. The improvement of S and M_r/M_s was observed for the EB-deposited MgO samples with a thick MgO layer.

Acknowledgments

This work was partly supported by a Grant-in-Aid from the Japan Society for the Promotion of Science and the Ministry of Education, Culture, Sports, Science and Technology, by the New Energy and Industrial Technology Development Organization, and by the Strategic International Cooperative Program—Joint Research Type Japanese–German Joint Research in Japan Science and Technology Agency. The authors thank Dr. Takamichi Miyazaki for taking TEM images and helpful discussion.

1) X. Lou, C. Adelmann, S. A. Crooker, E. S. Garlid, J. Zhang, K. S. M. Reddy, S. D. Flexner, C. J. Palmstrom, and P. A. Crowell: Nat. Phys. **3** (2007) 197.
2) T. Uemura, T. Akiho, M. Harada, K. Matsuda, and M. Yamamoto: Appl. Phys. Lett. **99** (2011) 082108.
3) S. Datta and B. Das: Appl. Phys. Lett. **56** (1990) 665.
4) M. Holub, J. Shin, D. Saha, and P. Bhattacharya: Phys. Rev. Lett. **98** (2007) 146603.
5) T. Seki, T. Shima, K. Takanashi, Y. Takahashi, E. Matsubara, and K. Hono: Appl. Phys. Lett. **82** (2003) 2461.
6) T. Seki, T. Shima, K. Takanashi, Y. Takahashi, E. Matsubara, Y. K. Takahashi, and K. Hono: J. Appl. Phys. **96** (2004) 1127.
7) A. Sinsarp, T. Manago, F. Takano, and H. Akinaga: Jpn. J. Appl. Phys. **46** (2007) L4.
8) M. Kohda, A. Ohtsu, T. Seki, A. Fujita, J. Nitta, S. Mitani, and K. Takanashi: Jpn. J. Appl. Phys. **47** (2008) 3269.